5.1 Introduction

Dyes are extensively consumed in various textile and fabric industries for product coloration due to their property of tolerating long-term intense exposure to sunlight and other environmental effects. More than 100,000 are dyes being used for industrial purposes, a considerable amount of which are also released with the effluent in the environment, which pollutes soil and water resources (Ratna and Padhi, 2012; Robinson et al., 2001). Complex chemical composition of dyes and their synthetic nature makes dyes impervious to color fading (Poots et al., 1976). Among these dyes, basic and azo direct dyes are considered to have soaring toxicity issues (Shore, 1996). Direct blue 199 (Fig. 5.1a), utilized for various purposes, has high visibility in water even at low concentration, and therefore, impedes sunlight and affects photosynthesis. The broad applicability of synthetic dyes (in textiles, papers, fabric, leather and cosmetic industries) is due to their fast coloring, efficient binding, tolerance to extreme environmental condition in addition to their numerous shades (Asilturk and Sener, 2012; Sajab et al., 2011; Wang et al., 2014). The diverse chemical composition and complex structures of these dyes, which give it an edge in application, is greatest threat to environment even at lower concentration as they are toxic, carcinogenic, mutagenic and teratogenic (Asilturk and Sener, 2012; Crini, 2006; Poots and McKay, 1976; Wang et al., 2014). The aquatic ecosystem is greatly being damaged as 10-20% of these dyes remains in the discharged effluents (Apkan and Hamid, 2009; Padhi, 2012; Robinson et al., 2001). The stringent regulation enforced by the countries in the recent past has compelled the researchers to look for the cost effective treatments of this complex natured dyes (Asilturk and Sener 2012; Daud et al., 2012).

Various conventional techniques being practiced for dye discoloration have issues related with time, cost, by-products (Kitajima et al., 2006) and higher stability of synthetic dyes (Tunesi and Anderson, 1987). In these methods, the pollutants are transformed to other phase, producing secondary pollutants rather than providing complete mineralization. Among physico-chemical treatments, adsorption proves to be the most favourable one (Asilturk and Sener, 2012; Wang et al., 2014). However the biggest disadvantage of this technique is transformation of one kind of pollutant to another kind (Kitajima et al., 2006; Tunesi and Anderson, 1987). To address this issue, advance technique such as ozonation, ultrasonication, oxidation, etc. has been tested for their efficacy in dye containing wastewater treatment (Byberg et al., 2013; Fuentes et al., 2014; Zhou et al., 2012). However, intermediates and secondary pollutants generated during these processes still pose a challenge to environment even after such advance treatments (Golob et al., 2005; Feng et al., 2012; Fersi and Dhahbi, 2008; Natarajan et al., 2011).

Advanced oxidation processes such as ultrasound (US) and O_3 , TiO_2 , UV , H_2O_2 and Fenton reagent and their combinations are efficient treatment method (Nidheesh et al., 2013). Application of ultrasonic irradiation in core experiments has been appreciated for its effectiveness in degrading the organic pollutants. Ultrasound waves, generated at very high temperature (5000 k) in this process carries chemical changes in aqueous solution which causes hemolytic cleavage of the H_2O within cavitation bubbles producing ^{o}OH and ^{o}H free radicals (Peller et al., 2003). These free radicals bring degradation of organic pollutants in the aqueous solution. Hazardous dye pollutants in effluent require complete mineralization (conversion into

H_2O, CO_2 and mineral acids) for safe disposal. However ultrasound-based degradation and mineralization does not approach an appreciable extent due to several factors such as hydrophilic intermediate products and reaction volume (Muthirulan et al., 2014) which call for another efficient method for degradation of such stable and toxic chemicals.

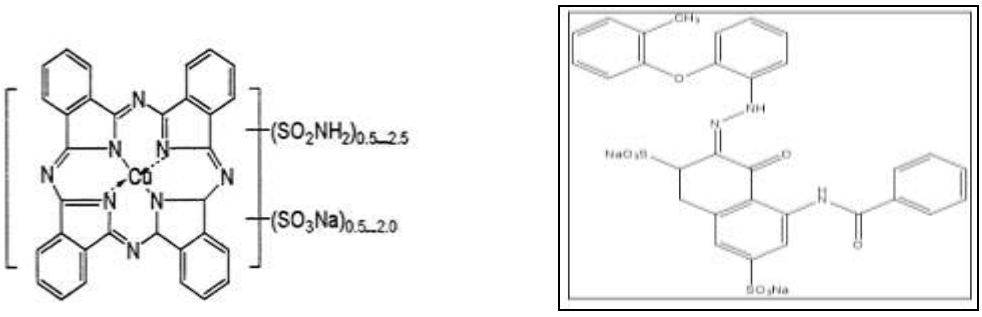

a **b**

Fig. 5.1: Molecular structure of two important dyes, (a) Direct Blue-199dye, and (b) Acid Red-131 dye.

Recently focus of the research community has been shifted to photocatalysis as it is proving to be available tool for the degradation of wide range of organic pollutants (Méndez et al., 2015; Seftel et al., 2015; Sood et al., 2015; Wang et al., 2015; Zhang et al., 2014). Low cost, non-carcinogenic oxidizing agent such as TiO_2 are being used for degradation of dyes under UV irradiation (Asilturk and Sener, 2012; Chong et al., 2009; Haque and Muneer, 2007; Ragupathy et al., 2015; Shao et al., 2013; Zhang et al., 2014). However, the major disadvantage of TiO_2 based catalysts is its low light utilization ratio as they exhibit increased activity only in UV range (anatase 3.3ev and rutile 3ev) (Wang et al., 2009). As a result, it shows photo-

catalytic activity only to a small fraction i.e., <5% of incident solar irradiation (Fuentes et al., 2014; Ragupathy et al., 2015; Romero et al., 1999). Therefore, this processes has been proposed to be made more effective by adapting either of two strategies viz., (1) utilization of cost-effective support materials such as activated carbon (AC) having high adsorption surface area, rapid adsorption kinetic and regenerability (Huang et al., 2011; Kitajima et al., 2006), and (2) by doping of semiconductors such as graphene to make it active even in the visible range.

Semiconductor for the photo-catalytic activity (as it acts as electron carrier to inhibit the recombination of electron-hole pair) provides large contact (surface) area for enhanced photocatalytic activity (Wang et al., 2009). The rudimentary reason behind the mechanism of degradation by both photo-catalysis and sonolysis is the generation of ^{o}OH radical. Both processes bring mineralization of dyes into simple molecules of H_2O, CO_2, along with mineral salt etc. The combined effect of both processes (i.e., sono-photo-catalysis) allows for a greater degradation of these organic pollutants, though it uses more power as compared to individual processes. It is attributed to a synergistic effect between both these processes (Yu et al., 2009). Recent studies have shown that TiO_2/AC nano-composite enhance the oxidative activity of ultrasonic waves even in the absence of ultraviolet irradiation. The presence of this nano-composite during ultrasonication enhances the formation of acoustic cavitation bubbles whose explosion generates ^{o}OH radical, and hence, supports the degradation process (Garcia and Matos, 2010).

The TiO_2-activated carbon (TiO_2/AC) nano-composite, are generally prepared through sol-gel process, whereas the activated carbon is generally derived from low-cost wastes such as coconut shell, bamboo, vegetable fibres', corn shell, rice husk and bagasse (Ragupathy et al., 2015). The enhanced catalytic activity of TiO_2 with the addition of activated carbon might be due to: (1) inhibitory effect to recombination of free electron-hole pair, (2) more radiant energy due to large surface areas, and (3) involvement of hydrolysis and condensation reaction in processes (García et al., 2010; Huang et al., 2011; Zhang et al., 2014). Generally, the production of TiO_2/AC nano-composite is cheaper, viable and reproducible as per industrial requirements, as compared to other processes. In recent years, the degradation of dyes by the TiO_2/AC nano-composite has been appreciated as a reliable industrial process.

In the present chapter, degradation of two important organic dyes has been studied. Therefore, the work has been divided into two parts. Part (A, Section 5.4) will be dealing with the comparison of photo-catalysis, sonolysis and sono-photocatalysis processes for Direct Blue 199 dye degradation. Activated carbon using rice husk is prepared and used in the preparation of TiO_2/AC nano-composite at two different temperatures by sol-gel method. An elaborated reaction kinetics modeling for each process was done and the rate constants were compared. As the dye removal from effluent is a serious concern, the power consumption of three processes is compared for cost effectiveness. Further, the kinetic study of photocatalytic degradation of the dye is established considering the viability and cost-promising factors. Part B (Section 5.5) will be dealing with photodegradation of Acid red (AR-

131) dye stuff in the presence of activated carbon-TiO_2 nano-composite and its kinetic enumeration.

5.2 Material and methods: see Chapter 3 for more details.

5.2.1 Design of Reactors

Three reactors were used during the study (Fig. 2). A photochemical reactor which consists of a cylindrical reactor fitted-in with 8 Phillips UV lamps of intensity of 960 Lux along with a magnetic stirrer is used for photochemical degradation. Figure 5.2a shows schematic representation of the photochemical reactor. For carrying out sonication reaction a reactor fitted with a Sonicator (Hielsher Ultrasound Technology) was used as shown in figure 5.2b. Figure 5.2c shows a schematic representation of a reactor consisting of a combined sono- and photo-catalytic reaction. All these reactors were provided with cooling jackets with water flowing inside them to avoid overheating.

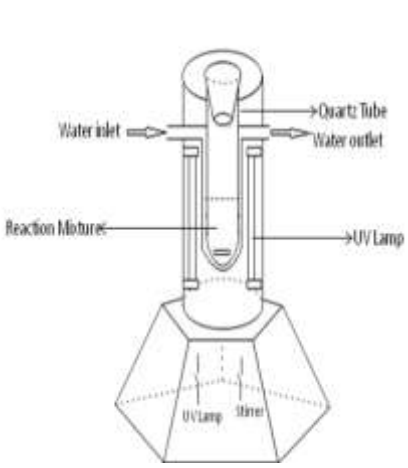

a

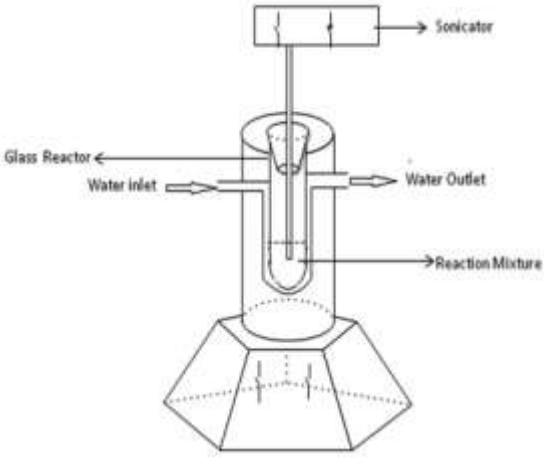

b

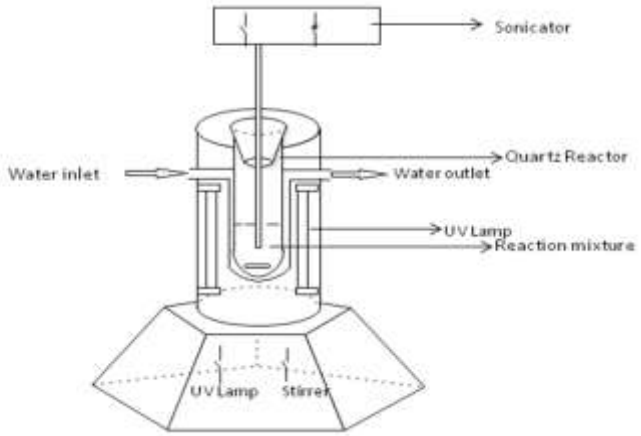

c

Fig. 5.2: Schematic representation of reactors used for the degradation of Direct Blue-199 dye: (a) Ultraviolet (photo) Reactor, (b) Ultrasound (sono) Reactor, and (c) Ultrasound-Ultraviolet (sono-photo) Reactor.

Various solutions consisting of different concentrations of dye, along with TiO_2/AC nano-composite (catalyst) was used for the experiments. The experiments were conducted in the three reactors as shown earlier. The samples were taken out from the photo-reactor at fixed time interval and their concentration was measured. This data was then used for further deductions and calculations.

5.3 Results and Discussion

5.3.1 Characterization of catalyst

5.3.1.1 Brunauer Emmet Teller (BET) surface area Analysis

Specific surface area of samples of TiO_2/AC nano-composites was assessed using Brunauer Emmet Teller (BET) plot with relative pressure (p/p_0) ranging from 0.01 to 0.20. The sample calcined at the temperature 250 ^oC has a specific surface area (SSA) of 201.35 m^2 gm^{-1} as compared to the sample calcined at higher temperature of 350 ^oC whose specific surface area (SSA) was 288.70 m^2 gm^{-1}. Therefore, the heat-treatment temperature has large effect on the activity of TiO_2/AC nano-composites by changing its SSA, crystallinity, carbon residual, etc.

5.3.1.2 X-ray diffraction (XRD) analysis

X-ray diffraction analysis was performed to assay the phase composition and crystalline nature and size of prepared A.C/TiO_2 nanocomposites was used to identify the peaks of the sample by comparing with the standard data. Various Diffraction peaks as shown in (Fig.02). at 2θ=25.4°, 48.02°, 54.19°,62.72°, were given by A.C/TiO_2 nano composite which were assigned to (101),(200),(105),(103) reflections of anatase phase and peaks at 2θ=37.80°, being assigned to (210), reflects the rutile phase of TiO_2. The average intensity of rutile phase is considerably less as compared to that of anatase phase. Scherrer's equation can be used to determine the average crystalline size equation .

$$D = \frac{k.\lambda}{\beta.cos\theta}$$

Where, K= Scherer constant, λ= X-ray wavelength and β= the peak width of half maximum and θ= Bragg diffraction angle

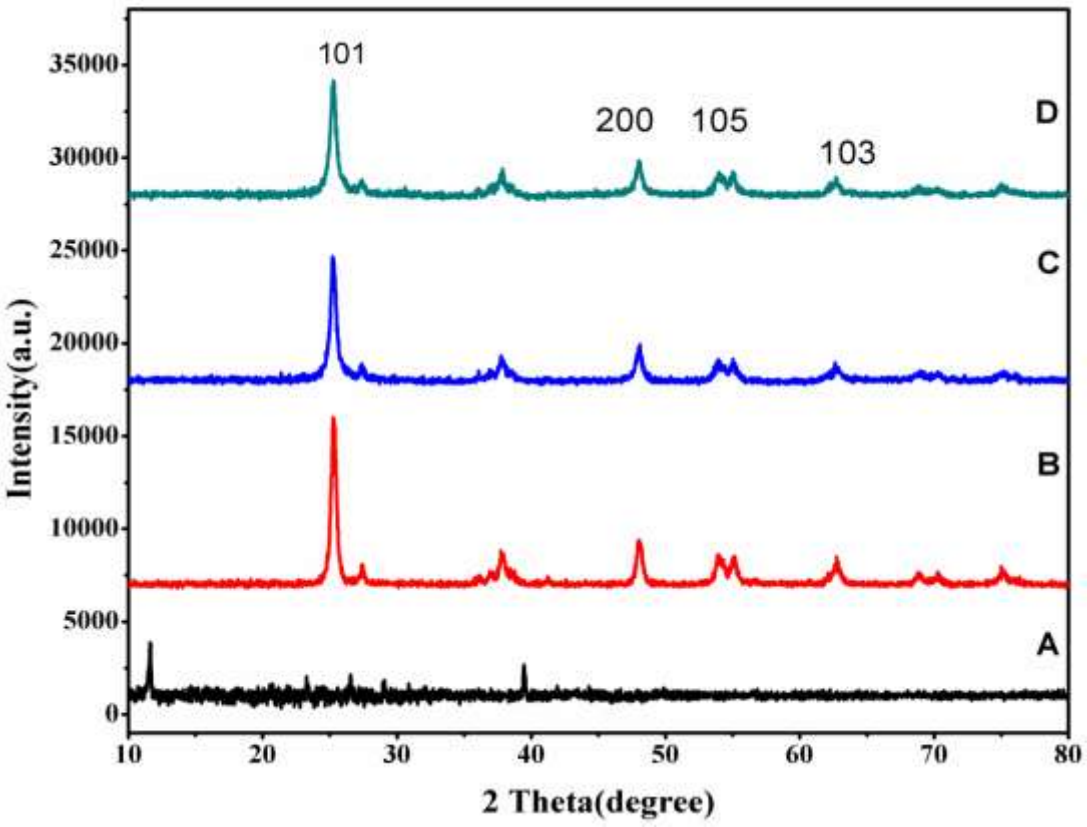

Figure 5.3: XRD spectra of (A) Activated carbon, (B) TiO_2, and (C) AC/TiO_2 Calcined at 250 ^oC and (D) AC/TiO_2 calcined at 350 ^oC

5.3.1.3 Scanning Electron Microscope (SEM) Analysis

The TiO_2/AC nano-composite was observed in scanning electron microscope (SEM) for investigating its surface characterization and structure. TiO_2 particle were clearly observed as dispersed and intertwined on activated carbon. The surface morphology of TiO_2/AC nano-composite is shown in Figure 5.4 a,b. The TiO_2

particles with the assessed diameter of about 22 nm enlaced and draped over the relatively large number of TiO_2/AC nano-composite (Fig. 5.4a,b) was in order.

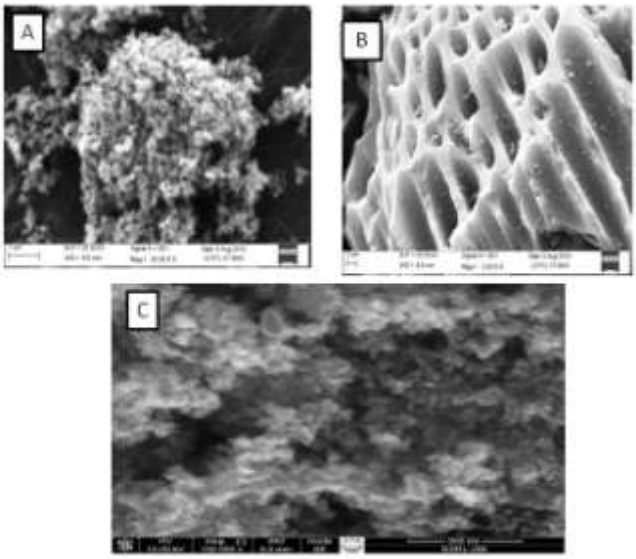

Fig. 5.4 (a): SEM images of (A) TiO_2 nanoparticle, (B) Activated carbon, and (C) TiO_2/AC nano omposite.

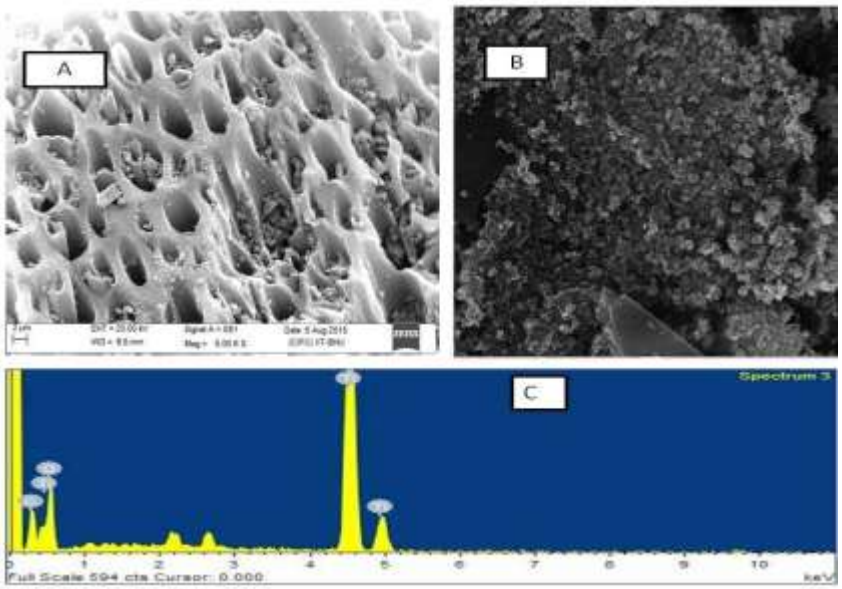

Fig. 5.4 (b): Scanning Electron Microscopy (SEM) Image of (A) Activated carbon (B) A.C/TiO_2 nano-composite (C) EDX spectra of TiO_2/AC.

5.3.1.4 FTIR Analysis

FTIR spectra of TiO_2/AC nano-composite give the number of peaks at different wave number (Fig. 5.5). Peak at 3415 cm^{-1} represents the stretching of hydroxyl (O-H) group in water as moisture (Abbad et al., 2012). Peak at 1632 cm^{-1} shows the stretching of titanium carboxylate, which was the product of TTIP and ethanol used in sol-gel method. Calcination of TiO_2 at higher temperature removes the hydroxyl and carboxylate peaks. Peak at 757 cm^{-1} represents the stretching of Ti-O bond which is the characteristic attribute of the formation of TiO_2 nano-particles. Because the AC absorbs whole IR radiation, description of its IR spectra is irrelevant. In addition, the hydroxyl group is not visible in AC's spectra (Hema et al., 2013). FTIR study of TiO_2/AC nano-composite shows the shift in the O-H vibration band towards lower wave number (3400 cm^{-1}) when compared to that corresponding to TiO_2. These shifts confirm the alteration of acid-base characteristics of OH group in the used samples (Singh et al 2015).

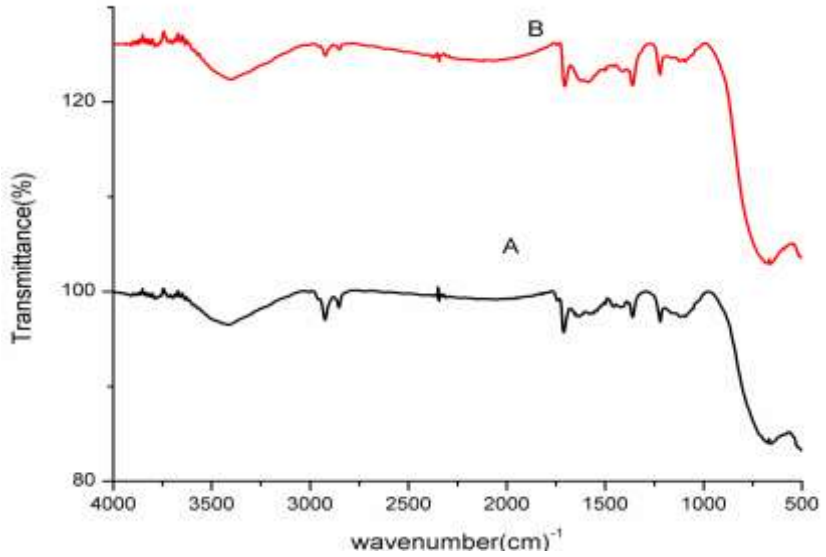

Fig. 5.5: FT-IR spectra of TiO_2/Activated carbon nanocomposite (A) after degradation, and (B) Before degradation of dye.

5.3.1.5 Raman Spectra analysis

Fig. 5.6 shows the comparison between the Raman spectra of activated carbon, TiO_2 nano particles and TiO_2 adsorbed on the surface of activated carbon. As per the observation, spectra of activated carbon (Fig. 5.6) exhibits two well-resolved bands, D (1332 cm^{-1}) and G (1585 cm^{-1}) which clearly indicates vibration C-C bond in activated carbon (Cuesta et al., 1994). Fig. 5.6 shows the Raman spectra of TiO_2 with each unit cell possessing tetragonal structure (Hyun et al., 2005). Raman spectra of single crystal indicates the four modes which appears at 133 cm^{-1}, 190 cm^{-1}, 386 cm^{-1}, 506 cm^{-1}, 630 cm^{-1} (Scepanovic et al., 2009). The first peak appearing at 133 cm^{-1} is slightly broader and shifted than those of a bulk TiO_2 crystal (Zang et al., 2000). As compared to short-range order of anatase phase in weak broader phase in high frequency region, certain degree of long-range order exists at 133 cm^{-1} peak (Arora et al., 2007). Fig. 5.6 shows the Raman Spectra of TiO_2/AC nano-composites having peaks at same wave number as that of spectra of TiO_2. The variation in intensity at given described peaks shows that activated carbon is successfully exfoliated and incorporated in the nanocomposite.

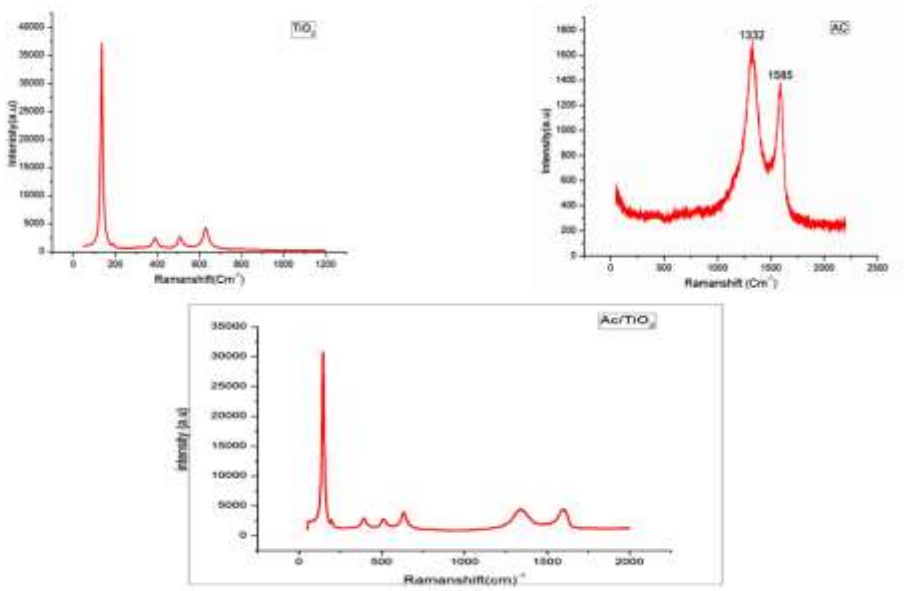

Fig. 5.6: RAMAN spectroscopy of (A) TiO_2, (B)TiO_2/AC nano-composites. and (C Activated C.

5.4 Photo-catalytic, Sono-catalytic and Sono-Photocatalytic Decolorization of Direct Blue-199 (DB-199) dye

5.4.1 Optimization of catalyst

Two photocatalysts were prepared by calcinating at two different temperatures, viz. 250 ^{o}C and 350 ^{o}C. Thereafter, a plot between concentration and time for a given sample of DB-199 was made. It could be easily inferred that catalyst calcined at 350 ^{o}C was more effective (as shown in Fig. 5.7) for a given set of reaction conditions under constant UV irradiation. This is due to the fact that at higher

temperatures the crystallinity is improved, and hence, increased the photo-catalytic activity.

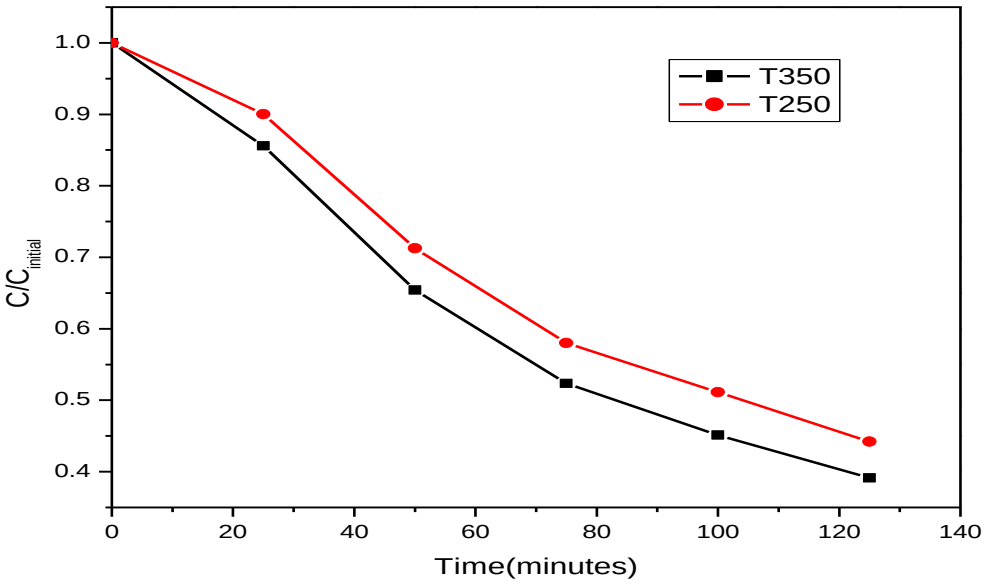

Fig. 5.7: Graph showing the change in Concentration vs. Time at two different calcination temperatures of the catalyst (250 ^{o}C and 350 ^{o}C).

5.4.2 UV-visible spectrum analysis of the dye

The maximum absorbance values were determined by scanning absorbencies in 200-800 nm wavelength range using a Systronics UV-Visible Spectrophotometer (Fig. 5.8). The maximum absorbance peak between 200 and 400 nm showed the aromatic content in the dyes while the peaks obtained in the range of 400-800 nm showed the absorption in visible range (Epling and Lin, 2002). This spectrum analysis result was used in determining the wavelength (λ = 635.4 nm) for optical density measurement.

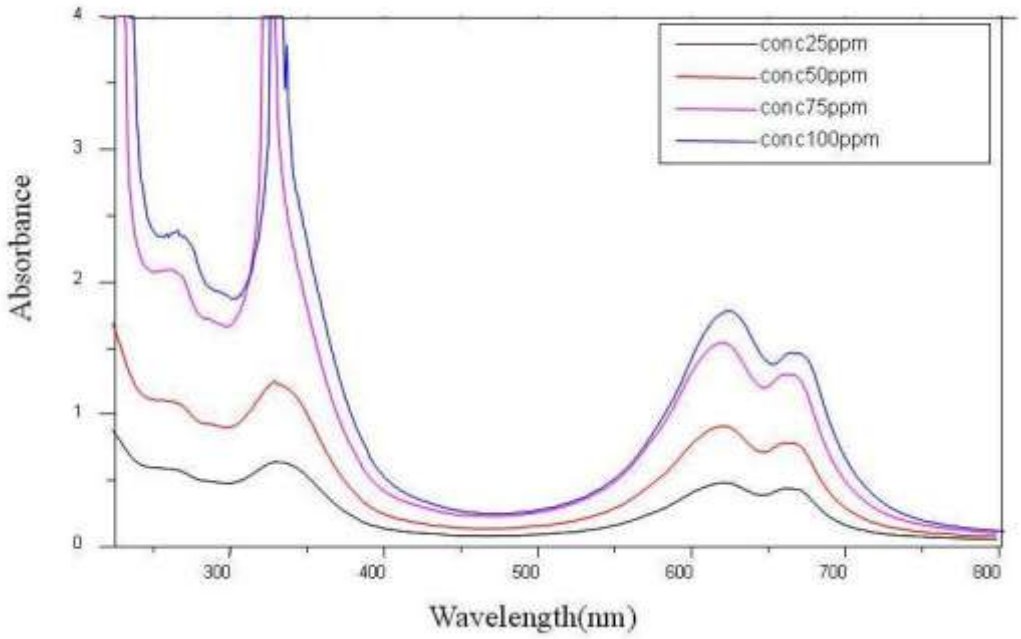

Fig. 5.8: Scanning absorbance of Direct Blue 199 (DB199) dye at various concentrations.

5.4.3 Photo-catalytic, Sono-catalytic and Sono-Photocatalytic Decolorization of dyes: Mathematical Modeling and Reaction Kinetics

5.4.3.1 Photo-catalyic decolorization of Direct Blue-199 (DB-199)

The reaction of DB-199 in presence of TiO_2/AC nano-composite and UV irradiation is an example of heterogeneous catalysis. Rate laws in such reactions seldom follow the proper law models, and hence, are inherently more difficult to formulate from the data. It has been widely accepted that heterogeneous catalytic reactions can be analyzed with the help of Langmuir-Hinshelwood (LH) Model (Lachheb et al., 2002; Matthews, 1988; Saien and Soleymani, 2007; Yang et al., 2011;

Zhang et al., 2000). With the following assumptions being satisfied: (i) there are limited number of adsorption sites on the catalyst and its surface is homogeneous, (ii) only one molecule can be adsorbed on one site and mono-layer formation occurs (as in chemisorptions), (iii) the absorption reaction is reversible in nature, and (iv) the adsorbed molecules do not react amongst themselves (Lachheb et al., 2002; Matthews, 1988; Saien and Soleymani, 2007; Yang et al., 2011; Zhang et al., 2000). According to LH Model following steps take place in the kinetics mechanism:

Step 1:

$$D(Dye) + C(catalyst) \leftrightarrow D.C$$

Adsorption of dye onto the catalyst surface

Step 2:

$$D.C \leftrightarrow E.C + Other\ Products$$

Surface reaction

Step 3:

$$E.C \leftrightarrow E + C$$

Desorption of products from the surface

A control experiment was first carried out under two conditions, viz., (i) Dye + UV (no TiO_2), and (ii) TiO_2 + Dye in dark (Fig. 5.9). It can be seen that under dark condition, after 25 minutes the amount of catalyst adsorbed becomes constant (i.e.

equilibrium adsorption is achieved). For the kinetic study of bleaching of DB-199, the initial concentration of dyes was varied and the experiments were first conducted in dark for 25 minutes, which was then immediately followed by UV irradiation (Fig. 5.10). The amount of catalyst was kept constant throughout the experiment (0.5 gm l^{-1}).

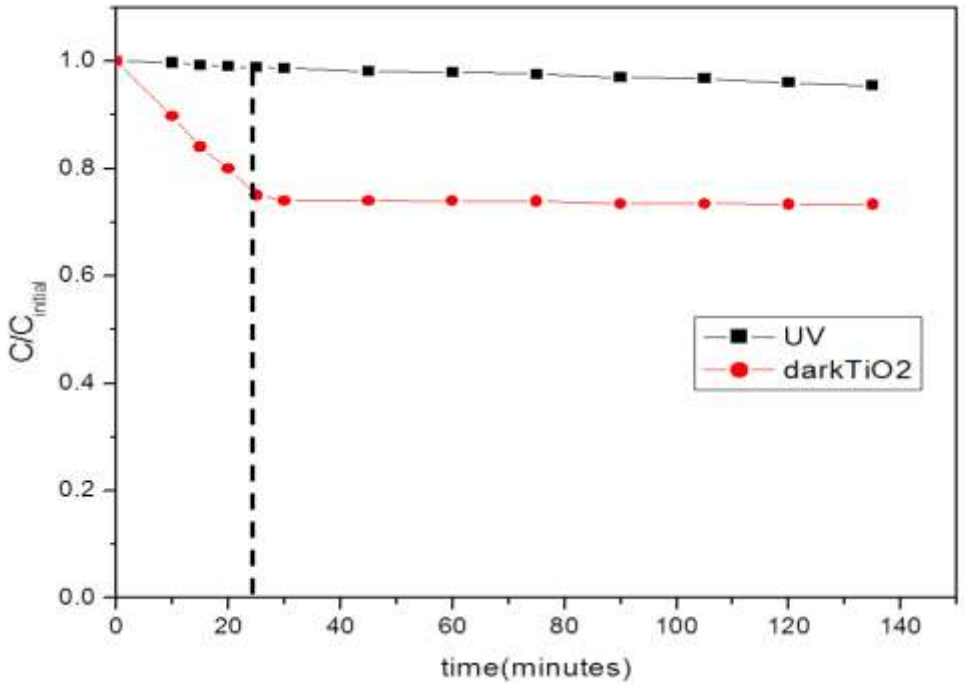

Fig. 5.9: Plot of change in concentration *vs*. time for (i) Dye + UV (ii) TiO_2 + Dye in dark.

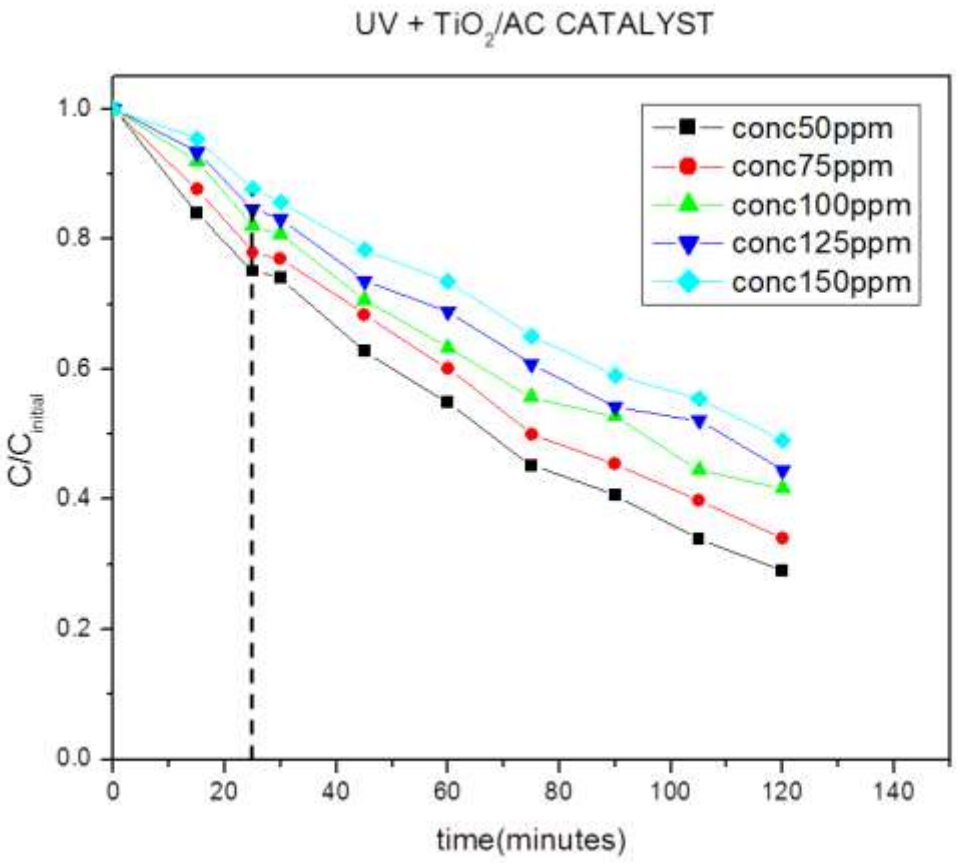

Fig. 5.10: Change in concentration of dye *vs*. time in presence of UV and TiO_2/AC nano-composite (The initial concentrations were 50 ppm, 75 ppm, 100 ppm, 125 ppm and 150 ppm).

5.4.3.1.1 Absorption of Dye onto the catalyst

Since the TiO_2 will be covered by both DB-199 (C) as well as water molecules (C_{water}) by hydrogen bonding, their competition for the active sites cannot be ignored. Langmuir's adsorption model can be applied to the aqueous solutions of dyes with the help of the following expression:

$$\theta = \frac{D_t}{D_{max}} = \frac{K_A.C}{1+K_A.C+K_{water}.C_{water}} \quad \text{(Eq. 5.1a)}$$

where θ is the fractional sites covered by the dye, D_t is the absorbed quantity of dye at any time, D_{max} shows the maximum quantity of dye that can be adsorbed, K_A is the Langmuir Adsorption constant for reactant, K_{water} is the adsorption constant for water. The value of $C_{water} \gg C$, hence C_{water} remains almost same throughout the reaction and the catalyst coverage by water molecules remains almost constant. Thus, we may ignore the quantity $K_{water}.C_{water}$ and rewrite equation 5.1a as:

$$\theta = \frac{K_A.C}{1+K_A.C} \quad \text{(Eq. 5.1b)}$$

The quantity adsorbed at a particular time can also be expressed as:

$$D_t = \frac{(\text{Reactor Volume}) \times (\text{Change in Concentration})}{\text{Mass of catalyst}} \quad \text{(Eq. 5. 2)}$$

The equilibrium adsorption quantity D_{eq} can be written as:

$$D_{eq} = D_{max}\left[\frac{K_A.C_{eq}}{1+K_A.C_{eq}}\right] \quad \text{(Eq. 5.3)}$$

where C_{eq} is the equilibrium concentration of the dye. On transforming equation 5.3, a function can be derived as follows: $\frac{C_{eq}}{D_{eq}} = f(C_{eq})$

$$\frac{C_{eq}}{D_{eq}} = \frac{1}{K_A.D_{max}} + \frac{C_{eq}}{D_{max}} \quad \text{(Eq. 5.4)}$$

From the figure 5.11, the intercept on the vertical axis gives $\frac{1}{K_A.D_{max}}$ and the reciprocal of slope gives D_{max}. The obtained parameters were tabulated as shown in Table 5.1.

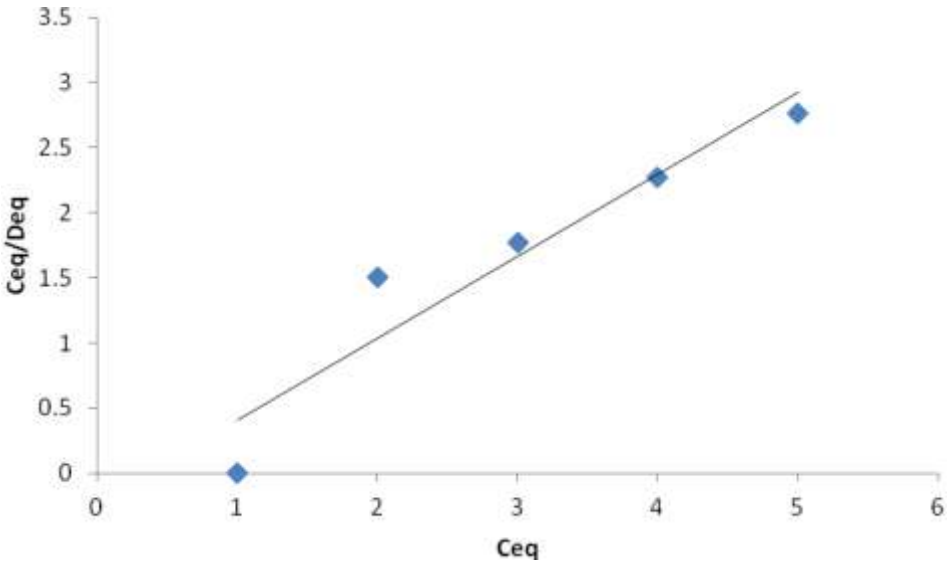

Fig. 5.11: Plot showing the linear variation of reciprocal of initial rates *vs.* reciprocal of initial concentration.

5.4.3.1.2 Photocatalytic degradation

Applying the Langmuir-Hinshelwood model for determining the oxidation rate of the photocatalysis of dye:

$$Rate\ (r) = -\frac{dC}{dt} = k.\theta = \theta = \frac{k.K_A.C}{1+ K_A.C} \quad \text{(Eq. 5.5)}$$

where k is the rate constant (mg l^{-1} min^{-1}), C concentration of dye, K_A is the adsorption constant of the dye (l mg^{-1}), t is the illumination time (minutes).

During the course of reaction, the initial pH, amount of catalyst and photo-intensity were kept the same. In addition, the formation of intermediates may interfere in the rate determination. Hence, the calculations were done at the beginning of UV irradiation. The rate expression can be written as:

$$r_o = \frac{k.K_A.C_o}{1+K_A.C_o} \quad \text{(Eq. 5.6)}$$

where r_o is the initial rate of degradation of DB-199, C_0 is the initial concentration (almost equal to C_{eq}). When the initial concentration $C_{initial}$ is very small, C_o will also be small and equation 5.6 can be simplified as a first order equation 5.7 and 5.8]:

$$-\frac{dC}{dt} = k.K_A.C_o \equiv ln\left(\frac{C_o}{C}\right) = k.K_A.t \quad \text{(Eq. 5.7)}$$

$$C = C_o.e^{-k_{f,photo}.t} \quad \text{Where} \quad k_{f,photo} = k.K_A \quad \text{(Eq. 5.8)}$$

The value of $k_{f,photo}$ can be determined from the plot of $ln\left(\frac{C_o}{C}\right)$ *vs.* t. The slope of the straight line obtained will be the value of first order rate constant. Table 5.2 shows the values of apparent rate constant for DB-199 degradation.

Obtaining a linear transformation from equation 5.6, we get: $\frac{1}{r_o} = f\left(\frac{1}{C_o}\right)$

$$\frac{1}{r_o} = \frac{1}{k} + \frac{1}{k.K_A.C_o} \quad \text{(Eq. 5.9)}$$

$$\text{Also } r_o = k_f.C_o \quad \text{(Eq. 5.10)}$$

Using equations 5.9 and 5.10, a linear regression of $\frac{1}{r_o}$ *vs.* $\frac{1}{C_o}$ was carried out and also a curve of r_o (initial rate) *vs.* C_o (initial concentration) was made. It can be clearly seen that initial rate of the reaction increases with the increase in initial concentration. Also the linear plot of $\frac{1}{r_o}$ *vs.* $\frac{1}{C_o}$ showed that L-H model is satisfied by the reaction. Thus, it can be said that in photocatalytic degradation of dye, initially adsorption of dye takes place and then degradation reaction (surface reaction) occurs.

The values of k and K_A obtained (from slope and intercept) were 1.135 min^{-1} and 0.016 l mg^{-1}, respectively. The value of K_A obtained from adsorption isotherm was not equal to K_A obtained from the L-H model. Ideally $[K_A]_{L-H} = [K_A]_{adsorption}$ but in this case $[K_A]_{L-H} = 0.414[K_A]_{adsorption}$. Various explanations have been attributed to this, such as: (i) adsorption occurs at the surface as well as in the bulk of the solution, (ii) non-homogeneity of the adsorption sites, (iii) adsorption of more than one molecule at one adsorption site, and (iv) deficiency of adsorption sites (Epling and Lin, 2002; Lachheb et al., 2002; Zhang et al., 2000).

5.4.3.1.3 Sonocatalytic and Sono-photocatalytic Decolorization of Direct Blue-199 (DB-199)

The change in concentration *vs*. time study was done for the other two reactors too *vis*. Sonocatalytic and Sono-photocatalytic as shown in (Fig. 5.12 and 5.13). The amount of catalyst taken was same as that for the photocatalysis reaction i.e. 0.5 gm L^{-1}. Both these reactions were assumed to follow the Langmuir-Hinshelwood Model.

The value of k_f (apparent Ist order rate constant) for each process was calculated using equations 5.11 and 5.12 (at different concentration of dye):

$$ln\left(\frac{C_o}{C}\right) = k_{f,sono}.t \quad \text{(Eq. 5.11)}$$

$$ln\left(\frac{C_o}{C}\right) = k_{f,sonophoto}.t \quad \text{(Eq. 5.12)}$$

where $k_{f,sono}$ and $k_{f,sonophoto}$ are apparent rate constants for sonocatalysis and sonophotocatalysis, respectively, and t is time in minutes.

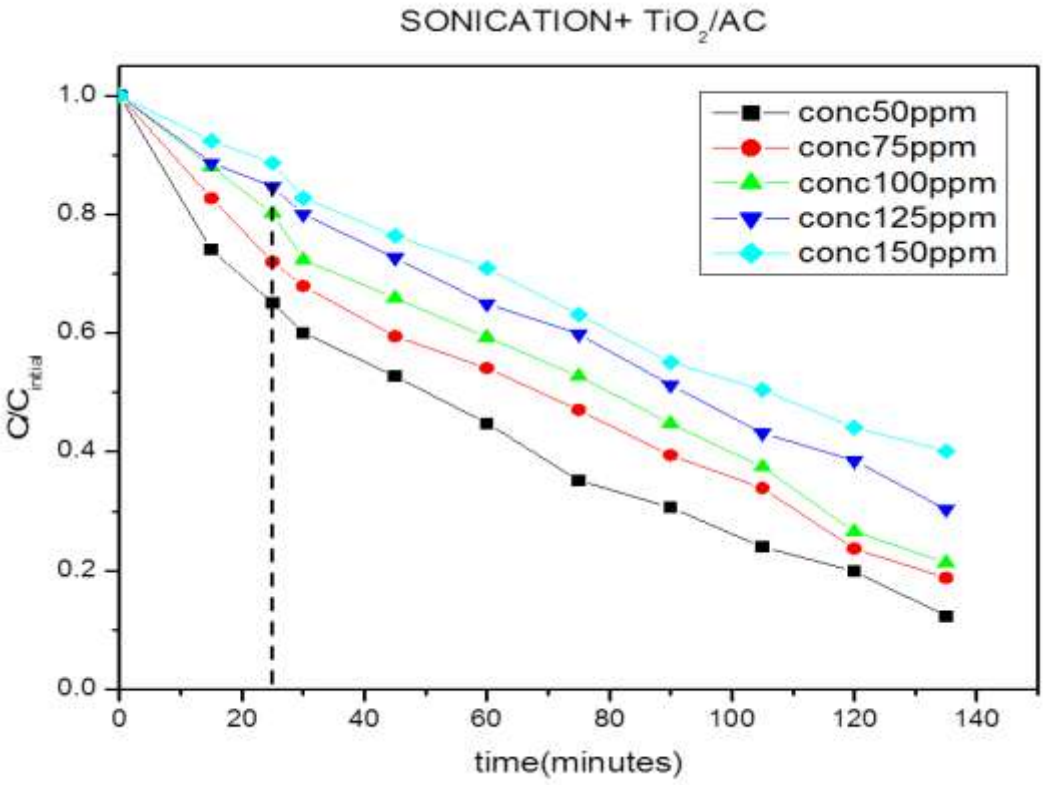

Fig. 5.12: Change in concentration of dye *vs*. time with sonication and TiO_2/AC (The initial concentrations were 50 ppm, 75 ppm, 100 ppm, 125 ppm and 150 ppm).

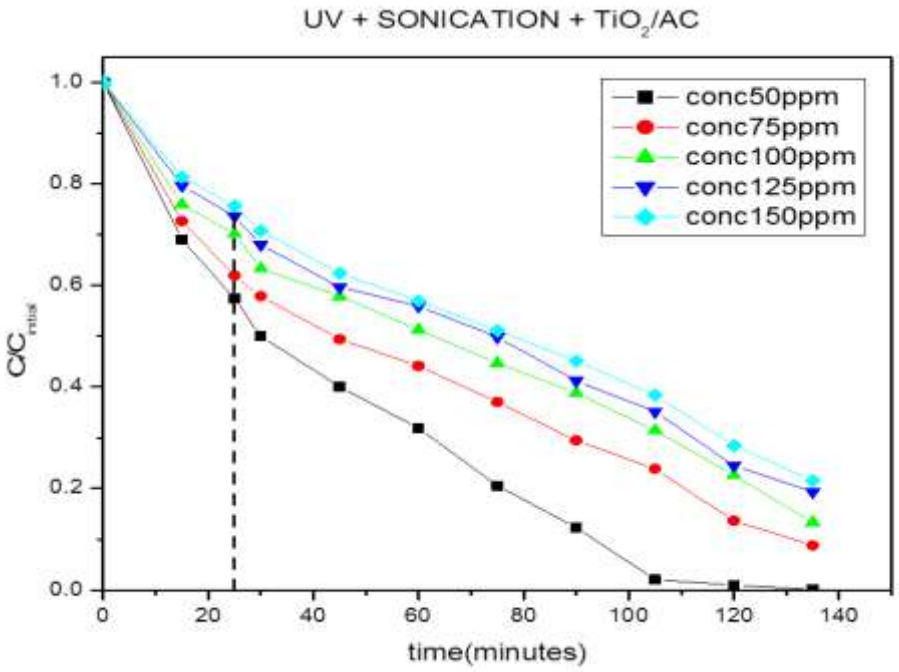

Fig. 5.13: Change in concentration of dye *vs.* time in presence of UV, Sonication and TiO_2/AC (The initial concentrations were 50 ppm, 75 ppm, 100 ppm, 125 ppm, 150 ppm).

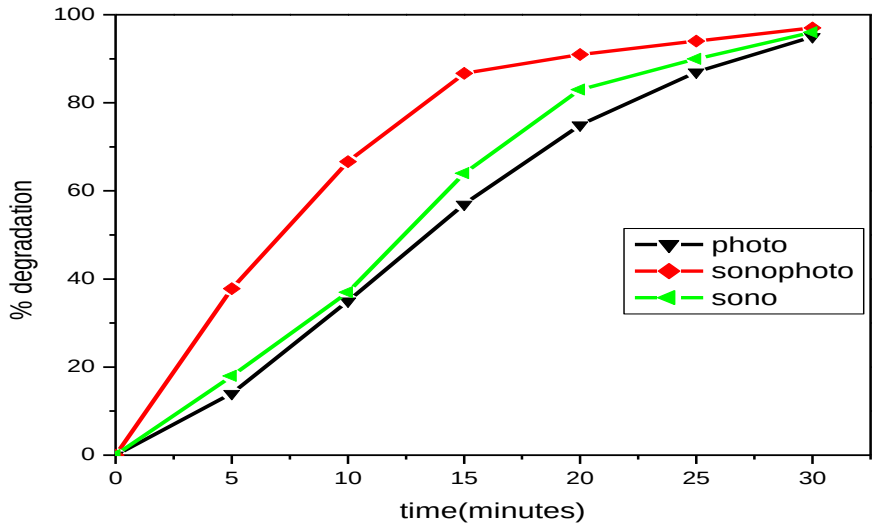

Fig. 5.14: Degradation (%) *vs.* Time for the photocatalytic, sonocatalytic and sono-photocatalytic reactors.

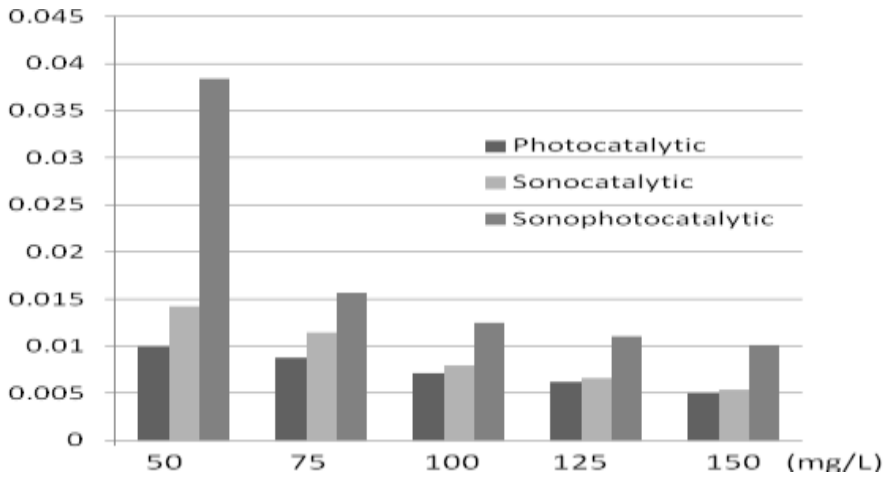

Fig. 5.15: Histogram showing the apparent First Order Rate Constants for the three reactors.

A comparative study was done as shown in figures 5.14 and 5.15. It can be seen clearly that rate constant of sonophotocatalysis was the highest followed by sonocatalysis and photocatalysis.

Thus, $k_{f,sonophoto} > k_{f,sono} > k_{f,photo}$

Table 5.1: The parameters of adsorption characteristics of DB-199: K_A (Langmuir constant), D_{max} (Maximum adsorbable quantity)

Parameter	Value
K_A (l mg^{-1})	0.03856
D_{max} (mg of dye gm^{-1} of catalyst)	45.8715
R^2	0.9796

Table 5.2: Value of apparent rate constant at various initial concentrations of dye solution for photocatalysis reaction

$C_{initial}$ (mg l^{-1})	k_f (min^{-1})	R^2
50	0.01001	0.9809
75	0.00876	0.9760
100	0.00712	0.9805
125	0.00623	0.9913
150	0.00512	0.9645

Table 5.3: The amount of energy consumed and the % degradation by the various reactors

Type of reactor	Total energy consumed (kJ)	Degradation (in %)
Photocatalytic	348	97 (in 30 minutes)
Sonocatalytic	660	94 (in 25 minutes)
Sono-Photocatalytic	763.2	98 (in 20 minutes)

5.4.4 Efficiency of the reactors

To determine which of the aforementioned processes is the most efficient, experiments were carried out at a particular concentration of dye (100 mg l^{-1}), and a higher concentration of catalyst (2 g l^{-1}). The reactions were conducted by three

different processes, viz. photocatalysis, sonocatalysis, and sono-photocatalysis. The % degradation *vs.* time plots were drawn for each (as shown in Fig. 5.14).

The Perkit India's photochemical Reactor (λ=185 nm), consisting of 8 Phillips (TUV 8W T5 G8) mini-lamps, with wattage 64W was used. The sono-catalytic reactor (Hielsher Ultrasound Technology) had an energy consumption of 440 J sec^{-1} and frequency 26 kHz. The combined reactor (sono-photo-catalytic) operated at wattage of 636 W. Comparing data in the table 5.3 and Fig 5. 16, it indicates that photo-catalytic reactor is the most economical on the grounds of overall efficiency.

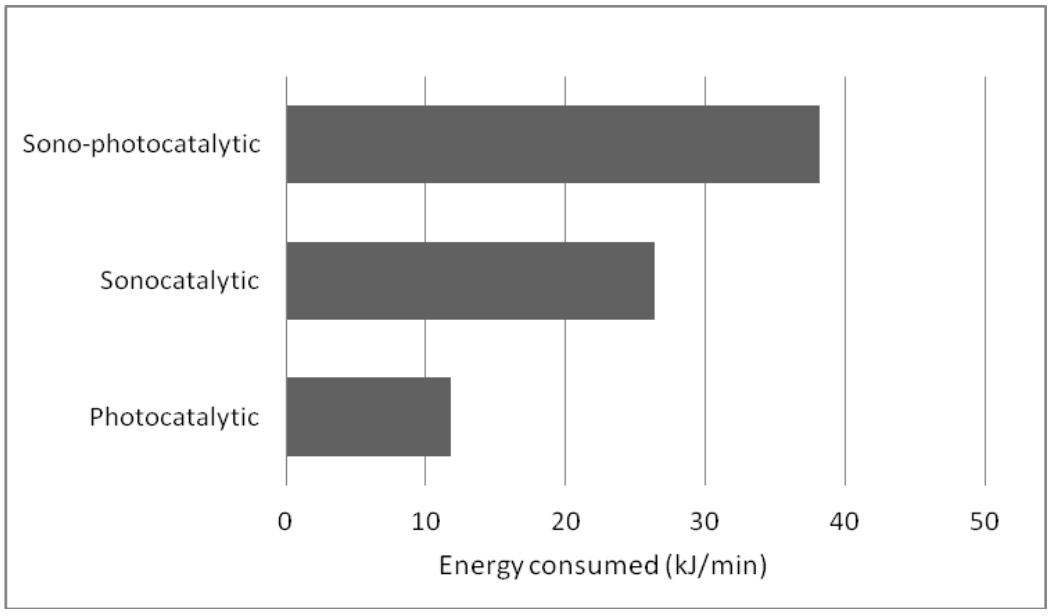

Fig 5.16: Graph showing the power consumption by photo-catalytic, sono-catalytic and photo-sono-catalytic reactors.

5.5 Degradation of acid red dye stuff in the presence of activated carbon-TiO_2 nano-composite and its kinetic enumeration

5.5.1 Degradation mechanisms and reaction kinetics

It has been found advantageous to study the heterogeneous catalysis reaction (such as Acid Red-131 dye + TiO_2/AC nano-composite) using Langmuir-Hinshelwood Model (Cunningham et al., 1994; Epling et al., 2002; Guettai et al., 2005; Lachheb et al., 2002; Matthews et al., 1998; Vautier et al., 2001; Vulliet et al., 2003). The main reasons for this are: (i) the resultant rate equation may be extrapolated more accurately to concentrations beyond the range of experimental measurements used, and (ii) the method considers the adsorption and surface reaction of the dye in a consistent manner. The L-H model is based on certain assumptions (Cunningham et al. 1994; Guettai et al. 2005; Vautier et al. 2001; Vulliet et al. 2003). Each active site adsorbs only one species of molecules:

A. The amount of adsorbed molecules has no effect on the rate of adsorption.

B. The extent of adsorption is never more than a monolayer.

On considering the degradation of Acid Red 131 as a single site mechanism, the L-H Model can be used to depict various steps involved in the degradation (Fig. 5.17). The dye molecules initially diffuse from the bulk of the solution to the catalyst and adsorb on its surface. The UV irradiation with photons of energy (>3.2 eV), more than the band gap of TiO_2, create holes (h^+) (in the valence band) and electron (e^-) (in the conduction band) pairs.

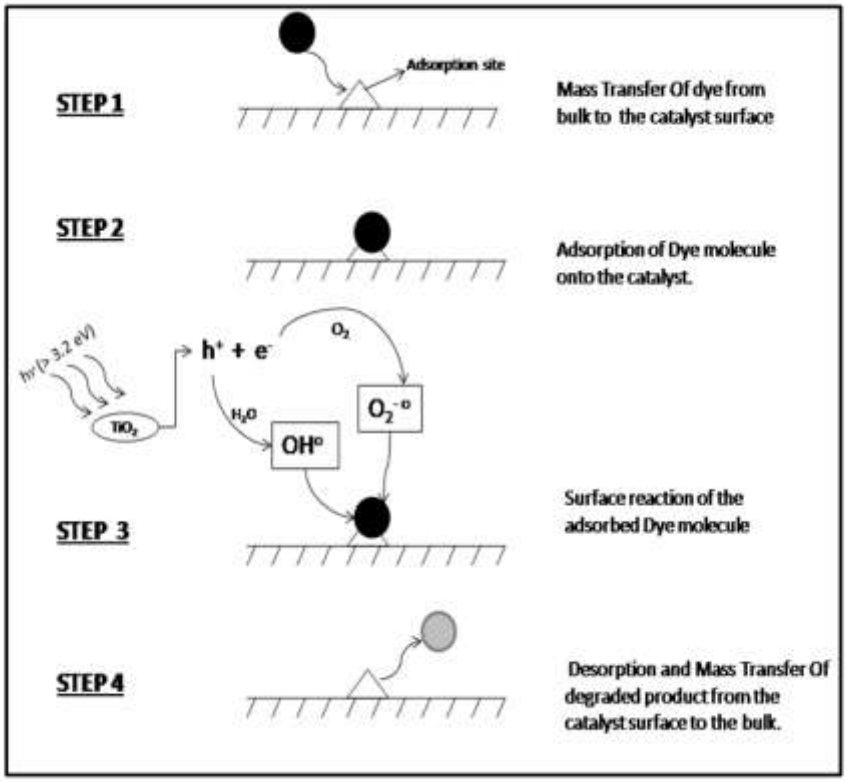

Fig. 5.17: Figure showing the proposed steps involved in dye (Acid Red 131) degradation.

The h^+ and e^- may bring respective oxidation and reduction of the dye molecule. Alternatively, the h^+ may react with OH^- or H_2O to form OH^o which in turn reacts with the dye molecule. Similarly, the e^- may react with the O_2 dissolved in water and convert it into superoxide radical (O_2^{-o}). The hydroxide radical (standard redox potential +2.8V) has the strong tendency to degrade the dye molecule. In this way, the photo-decomposition of dyes occurs in presence of TiO_2 (Bandara et al., 1999; Bianco-Prevot et al., 2001; Daneshvar et al., 2003; Galindo et al., 2000; Houas et al., 2001; Ioannis et al., 2004; Tanaka et al., 2000; Zhan et al., 1998).

I. $TiO_2 + UV\ (>3.2eV) \rightarrow h^+ + e^-$

II. $h^+ + H_2O \rightarrow OH^o + H^+$ or, $h^+ + A \rightarrow$ oxidized A

III. $e^- + O_2 \rightarrow O_2^{-o}$ or, $e^- + A \rightarrow$ reduced A

IV. $O_2^{-o} + H^+ \rightarrow HO_2^o$

V. $OH^o + A \rightarrow D$

(A: Un-degraded Dye Molecule; D: Degraded Dye Molecule)

(a) Equilibrium Adsorption

$$A + X \Leftrightarrow A.X$$

(A: Un-degraded Dye Molecule; X: Adsorption Site)

Initially, the equilibrium adsorption of a dye molecule (A) on to the adsorption site of the catalyst occurs. To study this adsorption, a control experiment was carried out in the dark (with no UV irradiation). The time required to achieve the equilibrium adsorption of dye on to catalyst was found to be 30 minutes (approx.) (Fig. 5.18A). This was followed by the UV irradiation of different concentrations of dye solutions, *viz.*, 25, 50, 75, 100 ppm at an optimized TiO_2/AC catalyst concentration of 0.5 g L^{-1} (Fig. 5.18B).

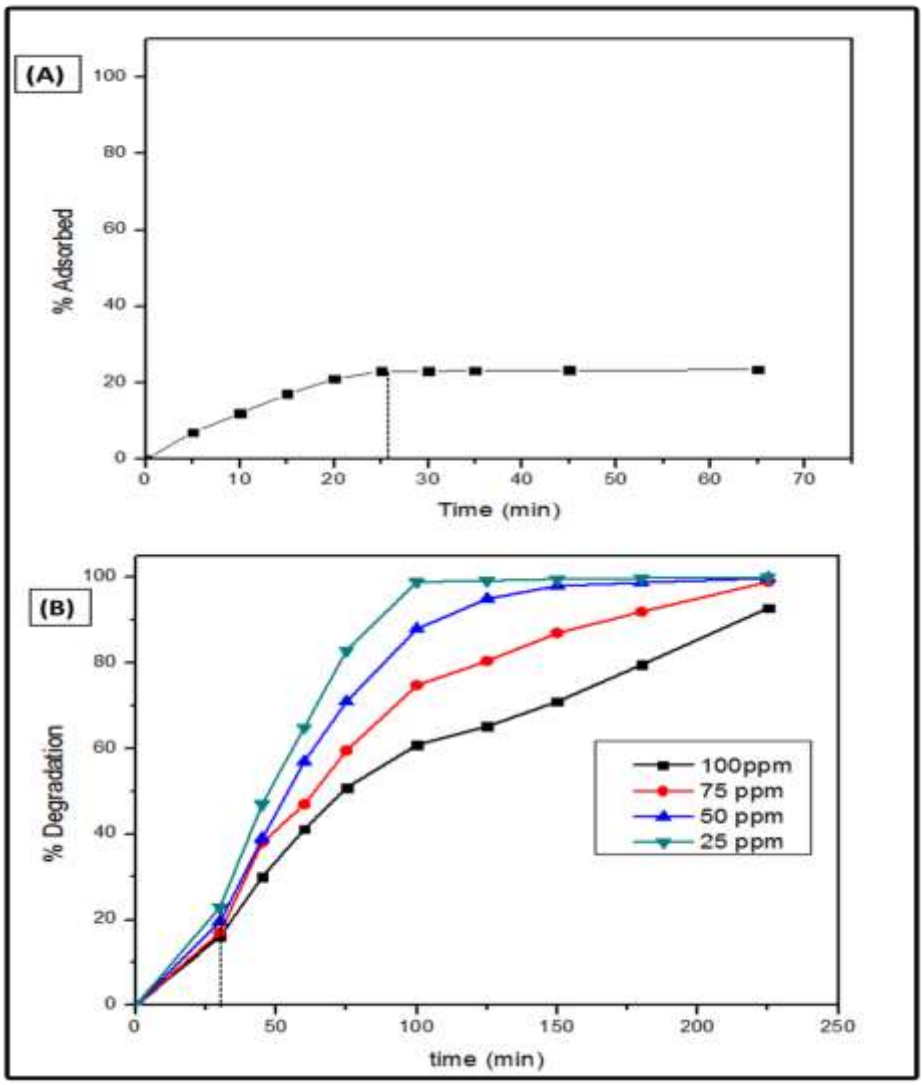

Fig. 5.18: (A) Figure showing the plot between % of dye adsorbed vs. Time (in dark conditions), (B) The degradation curves of Acid Red 131 dye solutions (of different concentrations) using TiO_2/AC catalyst.

On applying the Langmuir's Adsorption model to the adsorption of dye on to the catalyst surface the following equation can be written from the adsorption reaction:

$$k_a . C . \theta = k'_a . \theta' \quad \text{(Eq. 5.13)}$$

Equation 5.13 shows the equilibrium relationship of dye's adsorption. k_a and k'_a represents the forward and backward reaction rate constants for the adsorption of dye, respectively, C is the concentration of dye in the solution and, θ and θ' are the fraction of vacant and adsorbed sites on the catalyst, respectively.

Or $$K_a . C . \theta = \theta' \quad \text{(Eq. 5.14)}$$

Or, $$K_a . C . (1 - \theta') = \theta' \quad \text{(Eq. 5.15)}$$

Or, $$\theta' = \frac{K_a . C}{K_a . C + 1} \quad \text{(Eq. 5.16)}$$

K_a is the Langmuir Adsorption constant. Here, the adsorption of water molecules is ignored as its catalyst surface coverage almost remains constant throughout the reaction.

Also, $\theta' = {}^{A_t}/_{A_{max}}$ where A_t the number of molecules adsorbed at the surface in time t and A_{max} is the maximum number of molecules absorbable onto the catalyst. Thus, equation 5.16 can be rewritten for equilibrium adsorption as:

$$\frac{C_{eq}}{A_{eq}} = \frac{1}{K_a . A_{max}} + \frac{C_{eq}}{A_{max}} \quad \ldots \text{(Eq. 5.17)}$$

$$\text{And, } A_{eq} = \frac{(\Delta\text{concentration of dye}) \times (\text{Volume of reaction mixture})}{\text{Weight of catalyst}} \quad \text{(Eq. 5.18)}$$

The plot of $\frac{C_{eq}}{A_{eq}}$ *vs.* C_{eq} (Fig. 5.18) gives the various statistical parameters involved in Langmuir adsorption.

(i) $A_{max} = 66.67 \frac{\text{mg of dye}}{\text{gm of catalyst}}$

(ii) $K_a = 0.01 \frac{\text{litre}}{\text{mg}}$ ($R^2 = 0.9711$)

(b) Surface Reaction

$$A.X \Longleftrightarrow D.X$$

(D: Degraded Product)

The rate of bleaching of dye by photo-catalysis can be written using the L-H Model as follows:

$$\text{Rate } (r) = -\frac{dC}{dt} = k.\theta' \quad \text{(Eq. 5.19)}$$

Where, k is the rate constant (mg l^{-1} min^{-1}).

Using Equation 5.14, the rate expression can be expressed as:

$$\frac{r}{k.K_a.C} = \theta \quad \text{(Eq. 5.20)}$$

(c) Desorption of Degraded Product

$$D.X \Longleftrightarrow D + X$$

(D: Degraded Dye)

The equilibrium desorption equation can be written as follows

$$k_d.\theta_D = k'_d.C_D.\theta \qquad \text{(Eq. 5.21)}$$

Or, $$\theta_D = K_d.C_D.\theta \qquad \text{(Eq. 5.22)}$$

where, $K_d = {k_d}/{k'_d}$ and k_d and k'_d are the forward and backward desorption rate constant, C_D is the concentration of degraded product, θ_D is the fraction of catalyst surface covered by the degraded product.

Also, the sum of all the fractional sites coverage and the fractional vacant sites is unity as in Equation 5.23.

$$\theta_D + \theta + \theta' = 1 \qquad \text{(Eq. 5.23)}$$

Or, $$K_d.C_D.\theta + \theta + K_a.C.\theta = 1 \qquad \text{(Eq. 5.24)}$$

Or, $$\theta = \frac{1}{K_d.C_D + K_a.C + 1} \quad \ldots \text{(Eq. 5.25)}$$

Now from Equation 5.20 and Equation 5.25, we have:

$$\frac{r}{k.K_a.C} = \frac{1}{K_d.C_D + K_a.C + 1} \qquad \text{(Eq. 5.26)}$$

$$\text{Or,} \quad r = \frac{k.K_a.C}{K_d.C_D + K_a.C + 1} \qquad \text{(Eq. 5.27)}$$

Generally, desorption of the product is very fast, hence the factor $K_d.C_D$ can be ignored from the rate expression and the Langmuir-Hinshelwood (L-H) relationship is obtained Equation 5.28.

$$\boxed{r = \frac{k.K_a.C}{K_a.C + 1}} \qquad \text{(Eq. 5.29)}$$

As the concentration of dye used in the process is very low, the term $K_a.C \ll 1$, so it's also negligible. Hence, the final rate expression can be written as:

$$r_o = k.K_a.C_o \qquad \text{(Eq. 5.30)}$$

$$\text{Or,} \quad r_o = -\frac{dC}{dt} = k_f.C_o \qquad \text{(Eq. 5.31)}$$

$$\text{Or,} \quad \ln\left(\frac{C_o}{C}\right) = k_f.t \qquad \text{(Eq. 5.32)}$$

$$\text{Or,} \quad C = C_o.e^{-k_f.t} \qquad \text{(Eq. 5.33)}$$

where, k_f is the apparent first order rate constant, r_o is the initial rate of the reaction and C_o is the initial concentration at which the reaction begins (which is nearly equal to C_{eq} as the photo-catalysis of dye was carried out after the equilibrium adsorption was achieved). The value of k_f can be determined from the plot of $\ln\left(\frac{C_o}{C}\right)$ *vs.* t (Fig. 5.19). The slope of the straight line obtained will be the value of first order rate constant (Fig. 5.19).

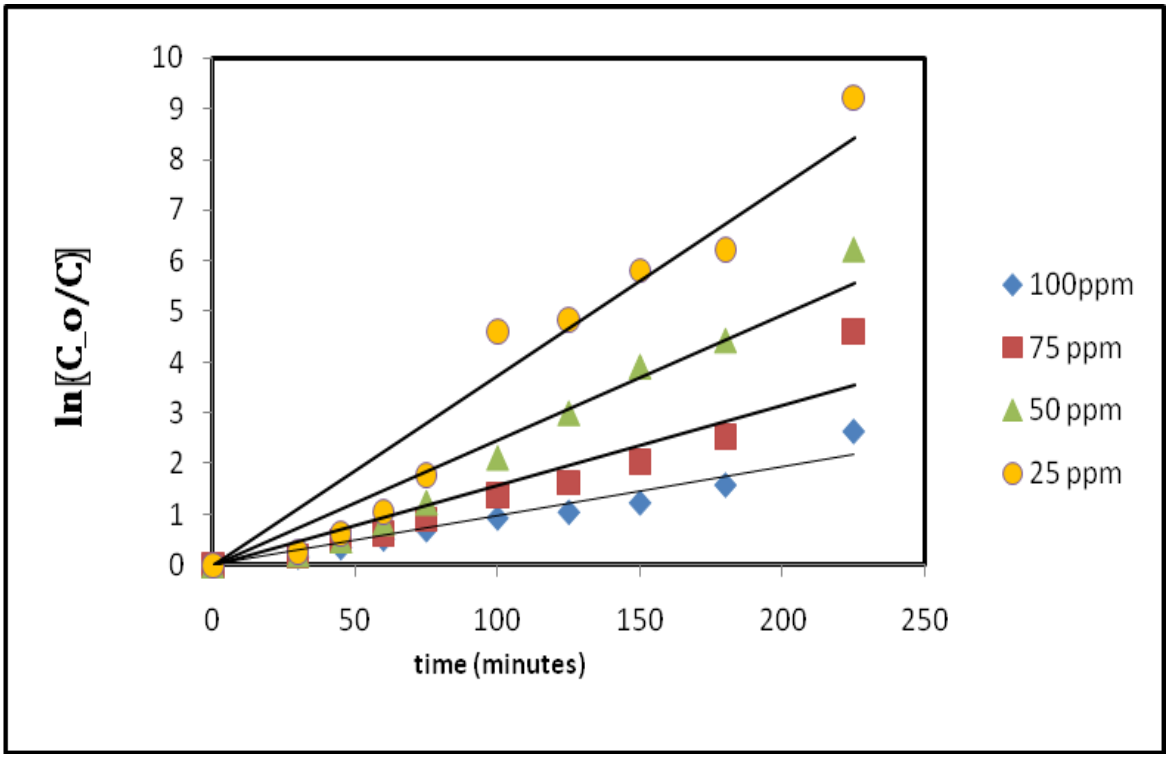

Fig. 5.19: Plot of $\ln\left(\frac{C_o}{C}\right)$ *vs.* t at various concentrations (Slope = k_f (min^{-1}).

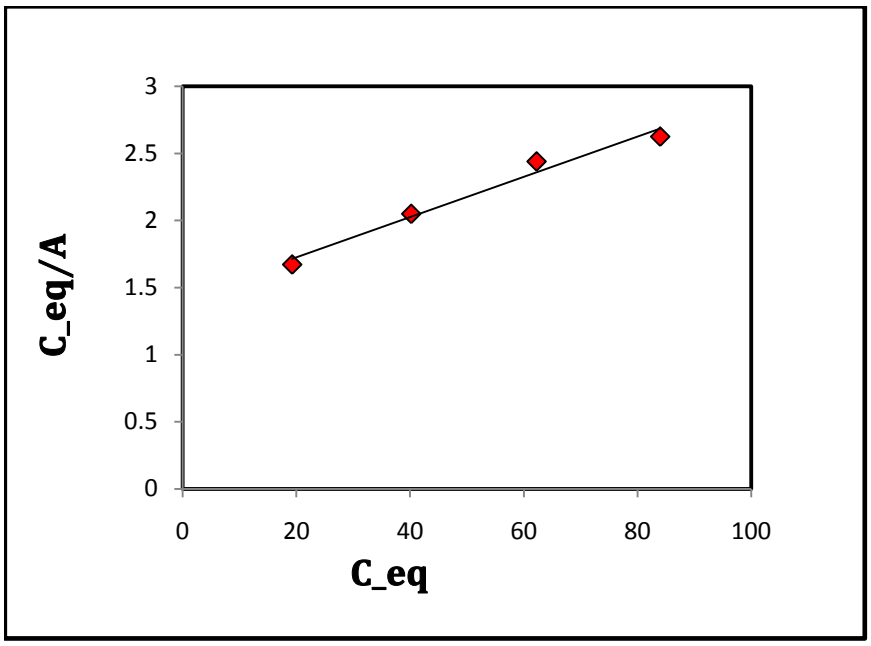

Fig. 5.20: Linear plot

A linear transformation of Equation 5.29 in terms of initial rate r_o can also be achieved as follows:

$$\frac{1}{r_o} = \frac{1}{k} + \frac{1}{k.K_a.C_o} \qquad \text{(Eq. 5.34)}$$

The (almost) linear plot of $\frac{1}{r_o}$ *vs.* $\frac{1}{C_o}$ (Fig. 5.20) shows that L-H model is satisfied by the reaction. Thus, it can be said that in photo-catalytic degradation of dye, initially adsorption of dye takes place and then degradation reaction (surface reaction) occurs.

Ideally, $K_{a,\ adsorption} = K_{a,L-H}$, but in this case $K_{a,\ adsorption} = 0.156K_{a,L-H}$, the reasons attributed to this are multilayer adsorption, non-homogeneity of adsorption sites and deficiency of adsorption sites (Cunningham et al., 1994; Lachheb et al., 2002; Vautier et al., 2001).

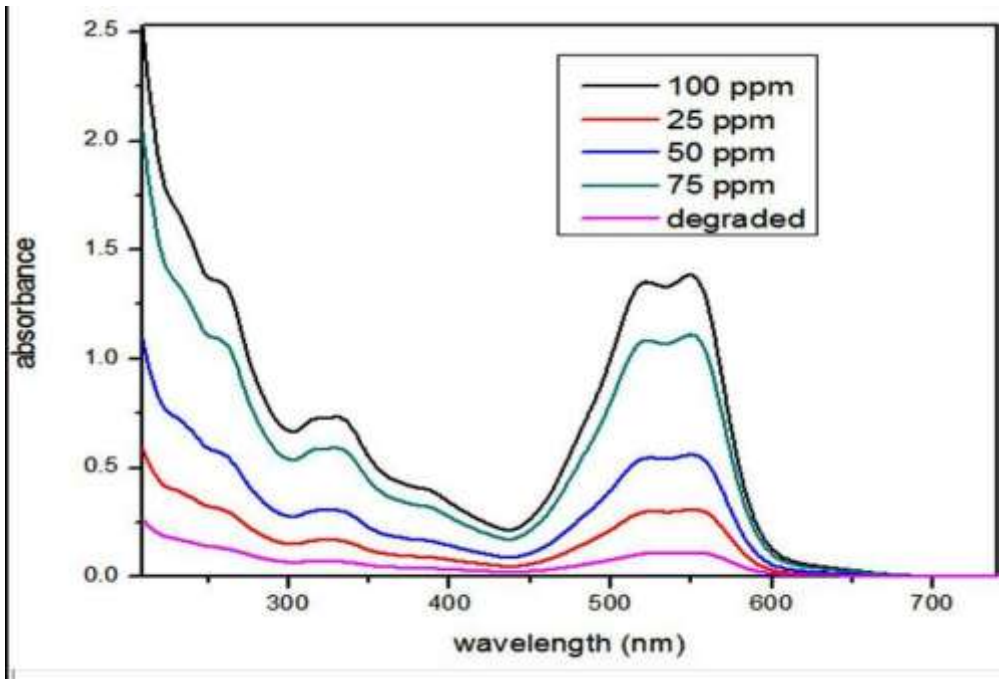

Fig. 5.21: Scanning absorbance of Acid red dye at various concentrations.

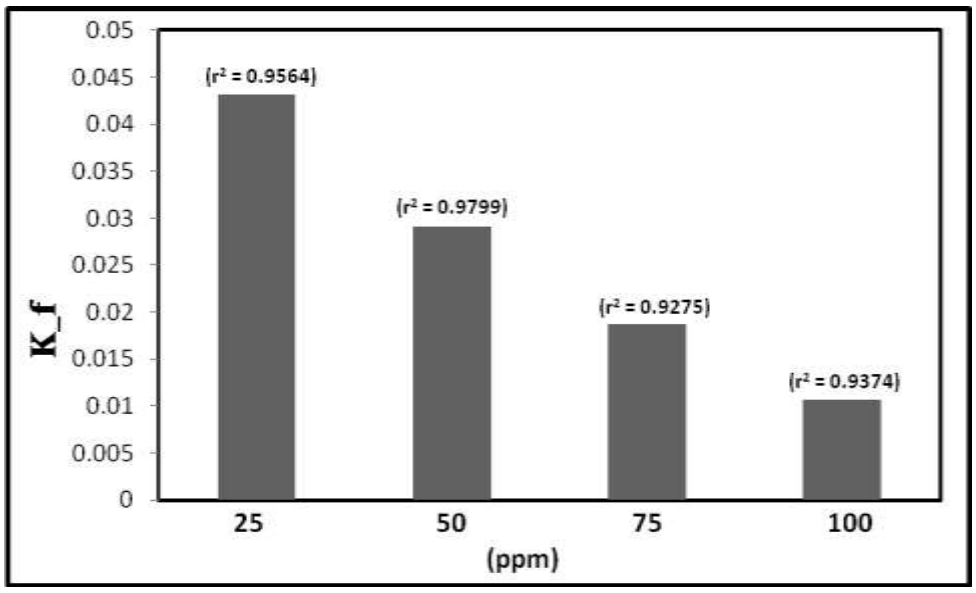

Fig. 5.22: Bar graph showing the values of first order apparent rate constants $\mathbf{K_f}$ for different concentrations of dye solution.

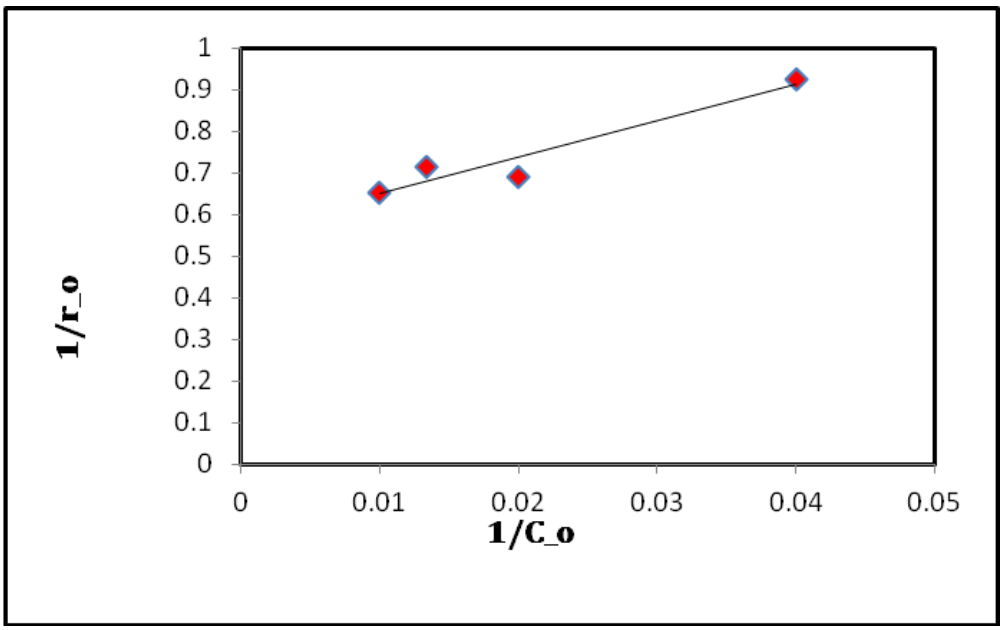

Fig. 5.23: Linear fitting of $\frac{1}{r_0}$ *vs.* $\frac{1}{C_0}$ (L-H Model), where $k = 1.775$ and $K_a = 0.064$ obtained from intercept and slope) (R^2= 0.981).

5.6 Conclusions

In this study, degradation analysis of Direct Blue-199 and Acid Red-131 dyes was done following various photo-catalytic pathways. A catalyst, TiO_2 loaded on Activated charcoal, was prepared in the process and its characterizations was done, which showed an even distribution of TiO_2 (rutile phase) on the catalyst surface. The catalyst calcinations temperature was also optimized, which was found to be ≈ 350 ^oC. A first order reaction kinetics was then developed for the catalytic oxidation of dye using L-H model. The degradation of DB-199, via photocatalytic, sonocatalytic and sono-photocatalytic reactions, under optimized working conditions followed L-H model satisfactorily. These three reactors used for the degradation of dye were tested on the basis of degradation rates and energy consumption. Photo-catalytic reactor was

found to be the best option amongst all the reactors used. The contribution of intermediates formed during the reaction is not considered in the kinetics study; however, there have been reports about the competitive involvement of intermediate products during the photochemical process. The role of intermediates can be involved further for the development of reaction kinetics model. After optimization of the reactor conditions and efficacy, degradation reactions of dye (AR-131) were done in the photochemical reactor. The degradation was found to follow a first order kinetics mechanism (viz., Langmuir-Hinshelwood Model).

*****